Spatially resolved absorption measurements of antimony atom formation and dissipation in quartz tube atomizers following hydride generation [☆]

Tomáš Matoušek [a,*], Magnus Johansson [b], Jiří Dědina [a], Wolfgang Frech [b]

[a]*Academy of Sciences of the Czech Republic, Institute of Analytical Chemistry, Laboratory of Trace Element Analysis, Vídeňská 1083, CZ-14220 Prague, Czech Republic*
[b]*Department of Analytical Chemistry, Umeå University, S-90187 Umeå, Sweden*

Abstract

The cross-sectional distribution of free antimony atoms generated from admission of stibine into quartz tube atomizers was measured by atomic absorption spectrometry. A CCD camera was used for the spatially resolved detection. In the unheated flame-in-tube atomizer, the highest free atom concentration was found near the tube axis, decreasing towards the walls. The free atom distribution was not influenced by atomization conditions such as purge gas flow rate and oxygen delivery. Significant changes in the free atom distribution were obtained by changing the position of the oxygen delivery capillary tip. Analyte reactions within the tube were revealed from an analysis of the curvature of the calibration curve. In the externally heated atomizer (900°C), the free atom distribution was much more homogeneous compared to the unheated atomizer under analytical conditions. However, pronounced inhomogeneity (higher concentration of free atoms near the tube axis and in the regions close to the walls) was obtained at high Sb concentrations in a roll-over part of the calibration curve (over 300 ng ml^{-1}). This is explained on the basis of free atom decay on the surface of polyatomic particles formed at high analyte concentrations. From a practical point of view, no effects caused by the inhomogeneous free atom distribution are to be expected in the heated 'flameless' tubes, the most widely used in routine analysis, since cross-sectional inhomogeneity observed under typical working conditions was negligible.   © 1999 Elsevier Science B.V. All rights reserved.

Keywords: Hydride generation; Spatially resolved atomic absorption; Quartz tube; Atomization mechanism; Sb

---

1. Introduction

At present, hydride generation-atomic absorption spectrometry (HG-AAS) is a simple, well established technique for the determination of hydride forming elements [1]. Basically, three types of hydride atomizers are available for AAS: diffusion flames, graphite- and quartz tube atomizers. Of these, quartz tubes are by far the most frequently used in virtue of their superior sensitivity and simplicity. Despite this, the processes taking place in quartz tube atomizers are still not fully understood.

Two versions of quartz tube atomizers are available: the flame-in-tube and the externally heated 'flameless' tube. In both types, hydrides are atomized in a cloud of hydrogen radicals [2,3], as has been confirmed by a number of independent investigations (see Dědina and Tsalev [1] and references therein). Hydrogen radicals are formed by the reactions of molecular hydrogen with traces of oxygen. The only important difference between the two atomizer types are the ways of H-radical formation: In the flame-in-tube atomizer, radicals are formed in a small flame at the end of the oxygen delivery capillary, whereas in the 'flameless' atomizer they are formed at the point where gases transporting the analyte species enter the hot zone of the atomizer. Sufficient oxygen is normally present as a contaminant. The cloud of hydrogen radicals is present in a small portion of the atomizer's volume. Free analyte atoms, generated in the H radical cloud, are transported by the flow of the purge gas to the atomizer bar-tube. Since free analyte atoms are thermodynamically forbidden outside the H radical cloud [1], they decay by chemical reactions, probably on the atomizer's inner surface. Once decayed, free atoms can be reatomized only by another source of oxygen forming H-radicals [4,5].

This concept of the processes taking place in quartz tubes was developed and verified mainly from studies on selenium- and arsenic-hydrides. Similar behaviour of antimony and arsenic described in Welz and Guo [6] permits broadening this concept to include antimony hydride atomization. It should be noted that recent findings indicate that the pathway for the atomization and decay of lead species is completely different, since free lead atoms can exist in thermodynamic equilibrium in quartz-tube atomizers [7].

Spatially resolved measurements have proved to be promising for the study of fundamental processes in analytical atomic spectroscopy, and are at present frequently utilised thanks to the progress in new technologies. So far, several approaches have been used for spatially resolved measurements in graphite furnaces. Holcombe and his co-workers [8,9] introduced a 'spatial isolation wheel' technique, permitting to observe defined parts of the atomizer's vertical cross-section during small time intervals. With this system, good one-dimensional and temporal resolution was obtained. Even the resonance schlieren method [10] was used to obtain one-dimensional resolution over the atomizer cross-section. By employing a laser-vidicon system, Huie and Curran [11] obtained two-dimensional resolution to monitor Na atom distribution over the entire atomizer cross-section. Two-dimensional resolution was also provided by the shadow spectral filming technique, developed by Gilmutdinov et al. [12]. They used a line source for illumination of the sample volume and a cine camera for detection. Later, the cine camera was replaced by a charge coupled device (CCD), providing improved sensitivities and versatile signal processing possibilities [13].

To our knowledge, two investigations involving spatially resolved measurements in quartz tube hydride atomizers have so far been made. Matoušek and Dědina [14] monitored the free Se atom distribution in an unheated flame-in-tube atomizer, using sequential measurements with a narrow, restricted beam from a line source in an AAS spectrometer. Various areas of the tube cross-section were monitored by adjusting the position of the atomizer. Lower densities of free atoms were found close to the tube walls. Johansson et al. [7] observed a nearly homogeneous distribution of Pb atoms in a heated quartz tube AAS system which was used as a gas chromatography detector. An optical system equipped with a CCD detector was used for spatially resolved measurements.

The aim of this study was to measure the cross-sectional distribution of free Sb atoms in a

quartz tube atomizer under various atomization conditions in order to elucidate possible mechanisms of free atom decay. A continuous flow hydride generation method, producing steady-state signals, was used, so there was no need for temporal resolution of the measurements. Antimony had been chosen for this investigation as a model hydride-forming element, mainly because this element has a resonance line at 231.2 nm. This is advantageous considering the decrease of quantum efficiency of our CCD towards short wavelengths, together with absence of strong emission lines in the neighbourhood of this line. Efforts to use this CCD to measure the free atom distribution of selenium, using the 196-nm line, were unsuccessful, as a result of insufficient resolution of the spectrometer and too low detector sensitivity at this wavelength.

2. Experimental

2.1. Reagents

All reagents were of analytical reagent grade or higher purity.

Standard solutions: 50–2000 ng ml^{-1} were prepared by dilution of a stock solution of 1000 μg ml^{-1} Sb (antimony potassium(+)-tartrate) with 1 mol l^{-1} HCl.

Blank solution: 1 mol l^{-1} HCl.

Reductant: filtered 1% (m/v) NaBH$_4$ solution in 0.4% NaOH prepared freshly each day.

2.2. Hydride generator

A compact, home-built continuous flow hydride generation system, shown in Fig. 1, was used. PTFE tubing (0.75-mm i.d. for liquid inlets and 0.5-mm for gas inlet) and T-pieces (PEEK — polyetheretherketone, 0.8-mm inner bore), connected by Rheodyne 1/16-inch flangeless fittings, were used throughout. Solutions and waste liquid were sucked by the three channels of a peristaltic pump. A gas–liquid separator was made from an open quartz tube, ending with a standard joint where it was closed by a quartz stopper with the gas outlet directed to the atomizer. It is possible to place a porous membrane, e.g. Teflon tape, at

the bottom of the connecting piece inside the standard joint to reduce spray entering the atomizer. However, such a membrane was not used in this work. The bottom of the gas–liquid separator is constructed from a rubber septum, through which passes a PTFE tube from the reaction coil and a PTFE tube for removing liquid to waste. The dead volume of the gas–liquid separator could be changed by moving the septum inside the tube but was kept at 3.0 ml throughout the experiments described here.

Peristaltic pump flow rates were 4.0 ml min^{-1} for blank and standard solutions and 1.1 ml min^{-1} for the reductant solution. In the hydride generator, 50 ml min^{-1} of hydrogen or argon was always used as the carrier gas. In most experiments, the carrier gas was mixed with an auxiliary gas in a T-piece downstream of the gas–liquid separator to obtain the desired atomization conditions. Purge gas flow rates given in the text include the carrier gas and also 30 ml min^{-1} of H$_2$ evolved by NaBH$_4$ decomposition.

2.3. Atomizers

Two quartz T-tube atomizers were employed: A laboratory made atomizer, designated as a dual mode atomizer, and a commercially available hydride atomizer from Perkin-Elmer's FIAS 200 system (designated as the FIAS atomizer).

The dual mode atomizer (Fig. 2) was 147 mm long and had a 10.5-mm i.d. The inlet arm (i.d. 4-mm) ended with a standard joint. This served for holding the delivery capillary for the intake of oxygen and, through a side arm of the purge gas and hydrides (see Fig. 2). The position of the capillary tip could be changed. In this work, if not stated otherwise, it was kept 10 mm inside the T-tube junction. This atomizer could be used in two ways: in the flame-in-tube mode (either heated or unheated) or in the 'flameless' mode (externally heated). In this case, oxygen was mixed to the purge gas in a T-piece upstream atomizer. The unheated atomizer can be used only in the flame-in-tube mode. For gas flows lower than 1100 ml min^{-1}, to prevent water condensation this 'unheated' tube had to be heated to 200°C using the furnace described below. If not stated
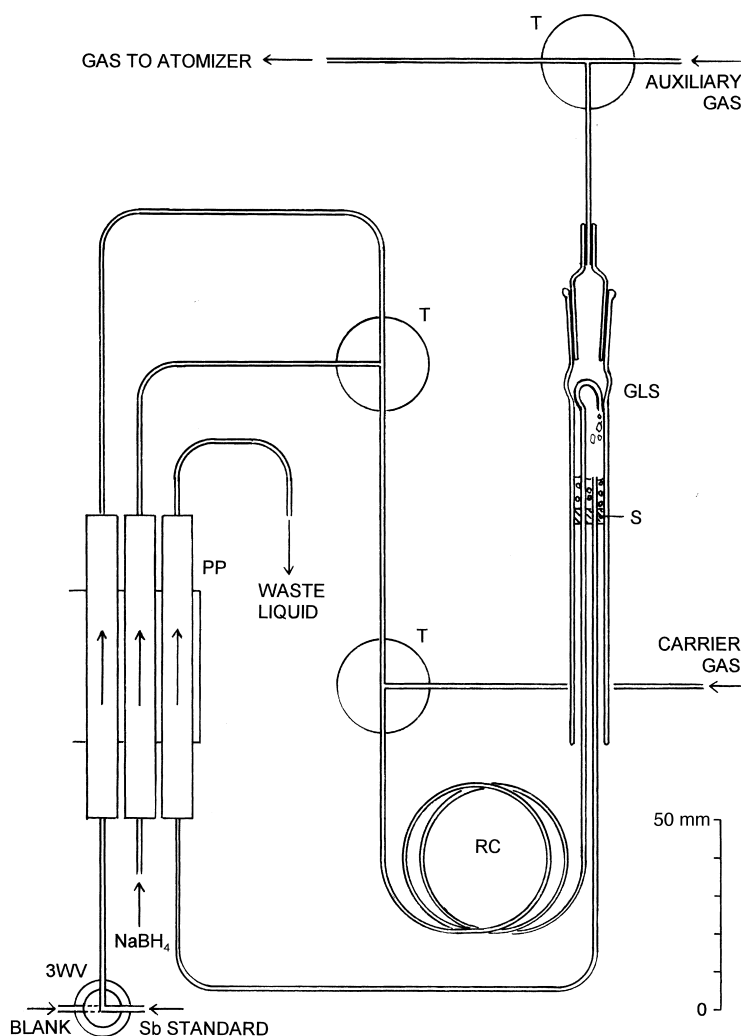
Fig. 1. Continuous flow hydride generation system. PP, peristaltic pump; T, T- pieces; 3WV, three way valve; RC, reaction coil, 1-mm i.d., 700-mm long; GLS, gas–liquid separator; and S, septum.

otherwise, the atomization conditions for the dual mode atomizer were: 2100 ml min^{-1} H$_2$ and 20 ml min^{-1} O$_2$.

The FIAS atomizer was 122 mm long with a 7-mm i.d. and provided with a straight inlet tube (i.d. of 1 mm) as described in Dĕdina and Welz [15]. The side windows were removed from this atomizer and it could be used only in the 'flameless' mode. For normal working conditions, 50 ml min^{-1} of purge gas (H$_2$ or Ar) were added to the 30 ml min^{-1} H$_2$ originating from NaBH$_4$ decomposition.

For external heating of either atomizer, a PC-controlled electrical furnace, kept at a set temperature of 900°C (Perkin-Elmer FIAS 200) was used.

2.4. Optical system

A schematic diagram of the optical set-up, used for the cross-sectional measurements of the density of Sb free atoms is depicted on Fig. 3. This set-up is slightly modified compared to that given in Johansson et al. [7]. The light from the primary
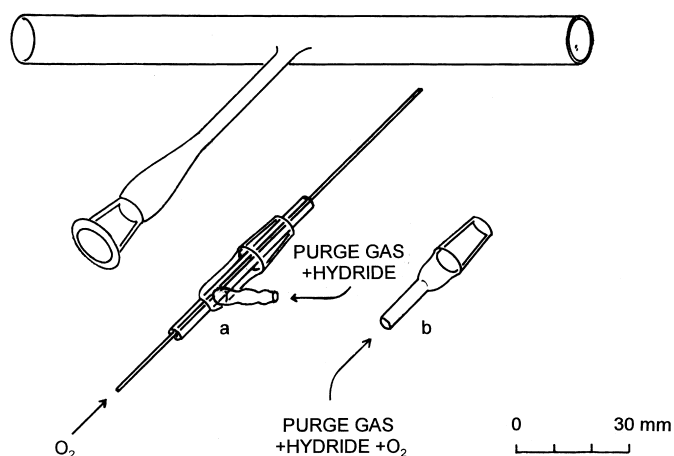
Fig. 2. Dual mode atomizer with intake parts for (a) flame-in-tube mode and (b) 'flameless' mode.

source (1), a Sb electrodeless discharge lamp (Westinghouse WL 40010) operated at 6 W, was directed by the biconcave quartz lenses (2) and (3) to illuminate the atomizer's optical bar (4). The aperture (5) restricted the visible part of the tube image (see below). The depth of field improving iris aperture (6) limited light entering the monochromator through the planconcave quartz lens (7). The monochromator (8) was a GM100 off-axis Ebert type with a grating of 1180 lines mm^{-1} and with a focal length of 100 mm, operated without slits. Dispersed images were projected on a Texas Instrument TC 241 CCD chip (9) of the camera (EDC-1000HR, Electrim Corp., Princeton, NJ, USA). The glass cover was removed from the camera to allow measurements of radiation at wavelengths below 350 nm. A PC

was used to control the operation of the detector and to receive the readouts. The software was written in C++ (Anders Jansson, Umeå University, Sweden), permitting sub-array scanning, i.e. a pre-selected part of the camera array could be scanned and stored on disk.

Measurements were performed in a dark room and before sample images were recorded solutions were introduced for approximately one minute to obtain a steady-state signal. Sample images consisted of the area illuminated by the light source and the 'dark' background regions outside the bright area. Typically, the procedure to obtain an image was as follows:. A blank solution was introduced to the hydride generator and a 'blank' image was taken and stored. Then, a Sb solution was introduced and a 'sample' image was
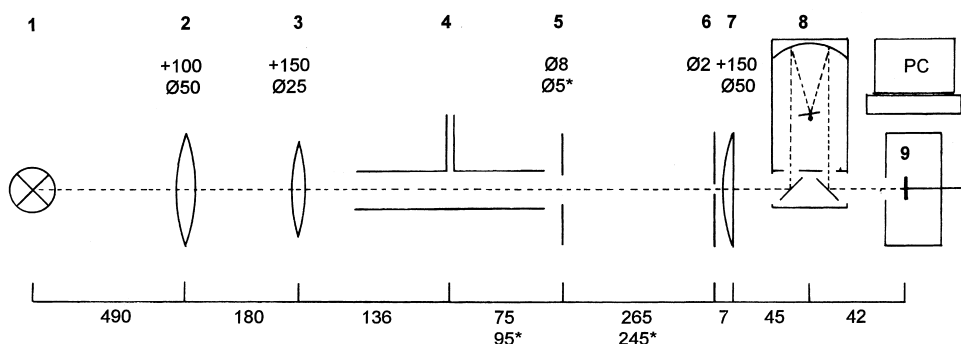

Fig. 3. Schematic diagram of optical setup for spatially resolved measurements in quartz tube. Distances, diameters and focal lengths in mm. See accompanying text for description. * For FIAS atomizer.

taken and stored. Both images were stored as matrix of 150×70 pixels depicting the 231 nm line image only, each pixel having a value between 0 and 255. Exposure times were 2500 ms and 4000 ms for the dual mode- and FIAS atomizer images, respectively. The exposure time and the size of the aperture (6) were chosen as a compromise between signal-to-background ratio and image sharpness. The response of the camera was checked to be linear within this integration time under pixel values of 180.

The data matrices were then processed in Matlab for Windows v. 4.2b software (The Math Works, Inc., Natick, MA, USA). For all matrix positions from the cross-section area of the atomizer the dark intensity, measured outside the atomizer image, was subtracted. The 100% transmittance image, I_0, was measured before the analyte measurement, I. The overall procedure was applied to correct for baseline changes as a result of unintentional alterations of optical components. The images present absorbance values based on individual matrix elements, and only that portion of matrix corresponding to the inside of the tube is shown. A few single pixels show no response due to failure of the CCD at these positions and these points have to be neglected in the evaluation.

To visualize the extent of cross-sectional inhomogeneity of Sb free atoms in a more explicit way, absorbances from a horizontal band over the image centre were plotted with selected figures (Fig. 6c and Fig. 10c, respectively). Absorbance values were obtained as the average value of 10 central elements for each matrix column in this case.

Single absorbance values (A_{mid}) presented in Fig. 5 were calculated as the average of absorbances of individual pixels in a square at the centre of the atomiser cross-sectional area covering approximately 20% of the total area.

3. Results and discussion

3.1. Spatial resolution

With the optical arrangement used, it was not possible to illuminate the entire atomizer com-

partment with completely parallel rays, as a result of the diffused spread of the emitted radiation. Selecting light from a smaller point would decrease the signal-to-background ratio, because of insufficient sensitivity of the CCD camera at the Sb wavelength. A schematic view of the presented images is given in Fig. 4a, together with the scheme of tube positioning. With the present optical configuration, the entire cross-section (10.5 mm in diameter) at the 'lamp' side of the optical bar was observed, but at the 'camera' side only the central part of the cross-section could be seen (7 mm in diameter). In other words, the more distant 'lamp' tube end appears smaller than the closer 'camera' end. Therefore, there was a blind region of maximum 1.8 mm thickness close to the tube wall at the camera side which decreased gradually to zero at the opposite tube end. This was confirmed by observing the shape of various screens and objects placed at different positions inside the tube. For the FIAS atomizer (7 mm i.d.), the situation was similar. This optical configuration is further referred to as the 'centre alignment'.

Obviously, the observed rays are parallel with the tube axis only in the centre of the image. With increasing distance from the image centre, the bias is increasing and different radial regions of the tube are probed over the tube length.

To be able to probe selected regions close to the tube wall over the entire tube length properly, the tube was realigned for some images, so that the part close to the wall at the near end matched the corresponding part close to the wall at the far end (Fig. 4b). In this case, the rays in the left-most part of the image (next to the wall) are parallel with the tube wall and sample the same radial position over the entire tube length. This configuration will be designated as 'wall alignment' (Fig. 4b), in contrast to the original 'centre alignment', when images of both ends are positioned concentrically (Fig. 4a). Only the proper half-images are presented in subsequent figures, as there is no relevant information in their other half. This inevitably non-ideal optical configuration will bias observed absorbance data. This error is, however, small for a homogeneously distributed atom cloud. To provide an estimate of
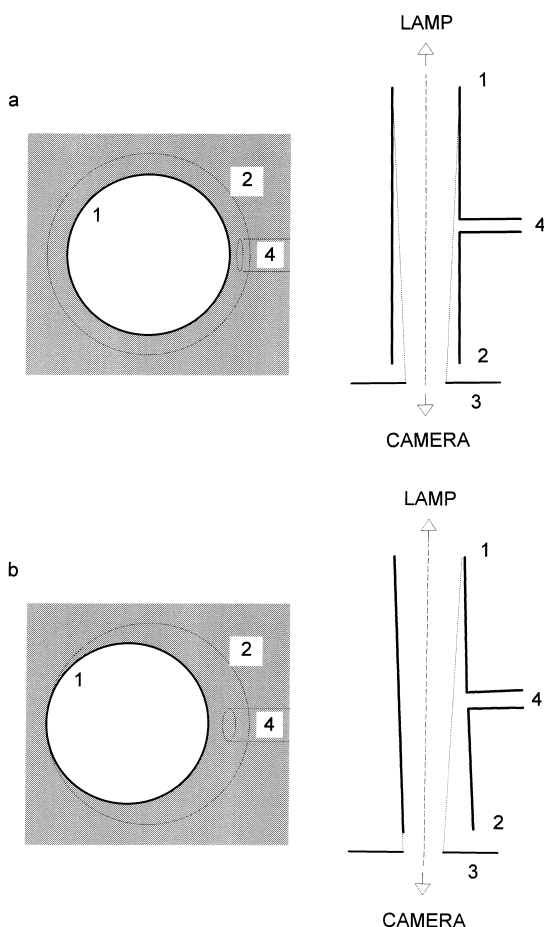
Fig. 4. Schematic description of the images with corresponding quartz tube position. (a) Centre alignment; (b) wall alignment. White area corresponds to the image. 1. Far (towards EDL) end of the tube aligned with the opening (3); 2. close (towards camera) end of the tube; 3. restriction aperture; 4. inlet arm.

the introduced errors, Fig. 6 shows CCD images for the same atomizer and sampling conditions, using wall and centre alignments. As can be seen, only minor differences in the apparent spatial distribution of atoms are present. By comparing the true thickness of a wire (0.5 mm), introduced at various positions in the tube, with its apparent thickness (it was derived from the wire image measurement relative to the tube image size to be 0.8−0.9 mm, independently of the point of insertion), the spatial resolution was assessed to be 0.2 mm over the entire tube length.

3.2. Spectral resolution

Tube images belonging to individual lamp lines were projected on the camera chip by selecting different wavelength regions. From the size and distance between the images for known wavelength intervals, the spectral resolution of the system was assessed to be 9 nm. The 231.1 nm Sb line was chosen for the measurements, as no strong emission lines were found in its neighbourhood. The 217.6 nm line could not be used as it was partially overlapped by relatively strong Sb non-analytical lines (214.0, 214.5, 220.1, 220.8, 222.1 and 222.5 nm).

Several weak lines were present within the spectral bandpass of the spectrometer even at the 231.1 nm line, but they did not interfere with the interpretation of the pictures. They could not be even traced in most of the images, as their intensity was less than 7% of the intensity of the resonance line.

Calibration graphs with the unheated dual mode atomizer (Fig. 5) were linear up to 0.4 when using the central part of the images (A_{mid}), as described in the experimental part. The curvature observed above this value is not caused by the non-homogeneous distribution of the free atoms over the cross-section of the atomizer, since the method of A_{mid} calculation yields the values independent of analyte cross-sectional distribution [16]. Curve bending, caused by an overlap of neighbouring non-absorbable lines constituting a total of 7% of the resonance line intensity, cannot alone explain the shape of the calibration graph. This is clearly seen from Fig. 5, where the solid line depicting the calibration biased by 7% of non-absorbable light is shown (its initial slope was derived from the first five experimental points). The experimental calibration bending would correspond to as much as approximately 20% of non-absorbable light (dotted line in Fig. 5). However, the presence of so much non-absorbable light was excluded. According to Gilmutdinov et al. [17], no calibration bending caused by spectral features from the Sb 231.1 nm line should be expected at absorbances around 0.6. The incomplete atomization at higher SbH$_3$ supply rates seems improbable, as lack of H-radicals in the
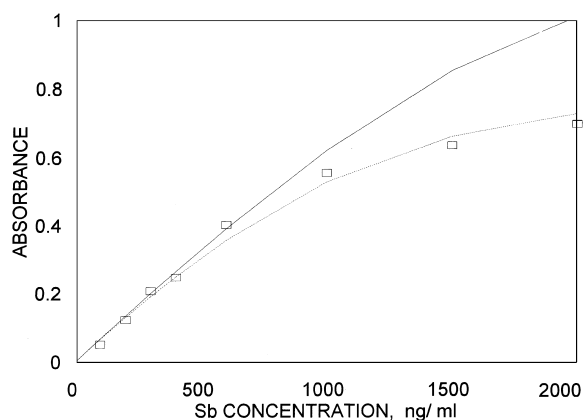
Fig. 5. Sb calibration graph in the dual mode atomizer based on A_{mid} values. Unheated flame-in-tube mode, 2100 ml min^{-1} H$_2$, 20 ml min O$_2$. Experimental points ($\square$) and calculated calibration curves assuming non-absorbable light of 7% (———) and 20% (.....) of the intensity of the analytical line.

flame-in-tube atomizer under analogous conditions has not been observed in an earlier interference study [1,14]. The obvious reason for the bending is thus an enhanced recombination of free Sb atoms in the gaseous phase at higher analyte concentrations.

3.3. Free Sb atom distribution in quartz atomizers

3.3.1. The unheated atomizer

As illustrated in Fig. 6, the cross-sectional distribution of free Sb atoms in the unheated dual mode atomizer shows similar characteristics to that previously observed for Se [1,14], i.e. the absorbance is highest in the centre and decreases

gradually towards the tube walls. The distribution is radially symmetric around the tube axis.

In separate experiments it was found that this distribution was little changed within the Sb concentration range of 100–2000 ng ml^{-1}, oxygen flow rate to the capillary of 10–50 ml min^{-1} or with an increase in distance of the capillary tip from the T-junction to 35 mm. All these results support the hypothesis that free atom decay occurs predominantly on the tube walls rather than within the atomizer free volume.

If the capillary is immersed into the optical tube, reaching almost the wall opposite the inlet arm (Fig. 7), it can be seen that most of the free atoms, formed by the flame, remain in the corresponding half of the cross-section, from where they slowly spread to the second half by diffusion. The inhomogeneity might be enhanced by an additional mechanism: traces of molecular oxygen can react with free analyte atoms, as recently proved for selenium [18] and lead [7]. Under normal atomization conditions, the oxygen traces are removed from the gas entering the atomizer when passing through the miniature flame burning at the end of the oxygen delivery capillary. However, when the capillary protrudes into the optical tube, not all the gas is passing through the flame so that more oxygen is present in the optical tube section close to its junction with the inlet tube. This causes fast decay of free atoms reaching this section. An analogous situation emerges when the oxygen delivery capillary is not centred in the inlet arm: more oxygen penetrates to the
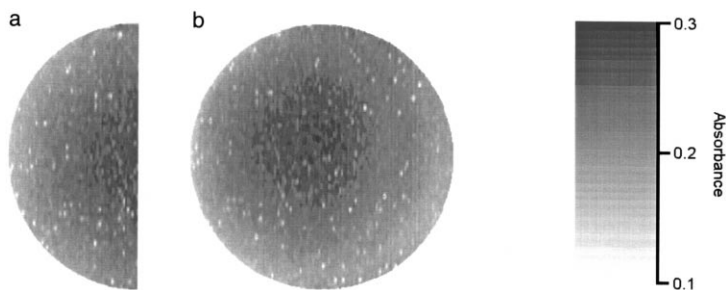

Fig. 6. Sb free atom distribution in the dual mode atomizer. Unheated flame-in-tube mode, 2100 ml min^{-1} H$_2$, 20 ml min O$_2$, 400 ng ml^{-1} Sb. (a) Wall alignment, (b) centre alignment; and (c) absorbance in the horizontal band 10 pixels wide over the middle part of the tube. (Figures 6 through 11 of this paper are available in colour as a supplemental file on the homepage of Spectrochimica Acta Electronica (http://www.elsevier.nl/locate/sabe). The figures are in a single archive under the name 'Spatial HG absorption of Sb in quartz tube' and identified by 05/631/99.
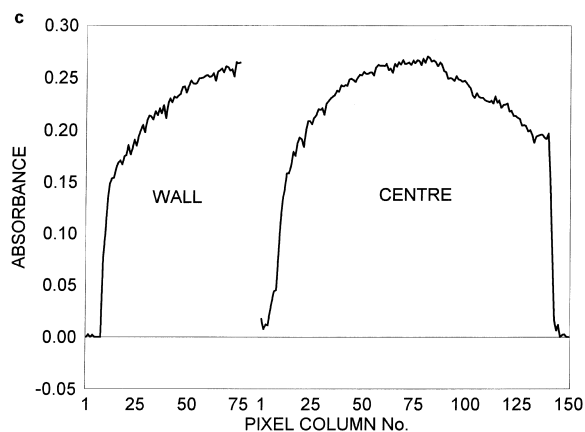
Fig. 6. *Continued*

optical tube causing a lower density of free atoms and a non-symmetrical profile (Fig. 8b).

Similarly, when decreasing the purge gas flow rate to the range 130–430 ml min^{-1} (capillary tip in standard position 10 mm from the tube junction), the atom distribution was highly inhomogeneous, being higher in the half cross-section close to the inlet arm (Fig. 9) in contrast to a perfectly symmetrical distribution at 2100 ml min^{-1} of H_2

gas flow shown in Fig. 6 and at 1100 ml min^{-1} of H_2 (not shown). A plausible explanation is the decay of free atoms on the inner atomizer surface opposite the junction [5]. The decay is much more pronounced here because of a higher probability of interaction of free atoms with the surface at low gas flow rates.

All these results show that substantial gas mixing on the way through the optical tube does not occur. Laminar gas flows prevail over most of the tube length, otherwise the cross-section atom densities would be homogeneous as a result of mixing by turbulent gas streams. Diffusion is therefore the main force transporting the free atoms towards the walls. This is in line with our previous observations [1,14].

3.3.2. The heated dual mode atomizer

When the atomizer optical tube is heated to 900°C, free atoms are distributed much more evenly over the atomizer's cross-section, probably as a result of an enhanced rate of diffusion. This is illustrated in Fig. 10 for the flame-in-tube mode, however, the 'flameless' mode yielded the same picture. The small decrease of the free atom
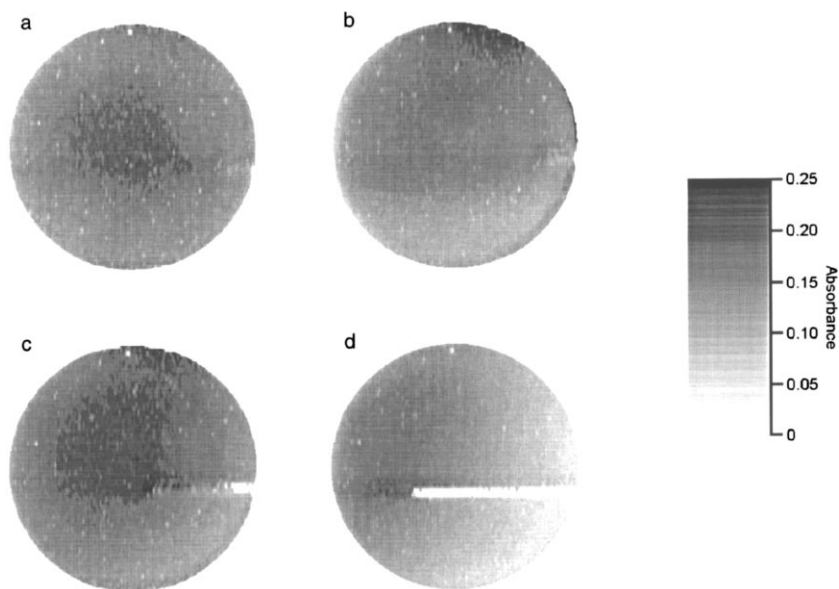

Fig. 7. Sb free atom distribution in the dual mode atomizer with the oxygen delivery capillary reaching into the optical bar. Unheated flame-in-tube mode, 2100 ml min^{-1} H_2, 20 ml min O$_2$, 400 ng ml^{-1} Sb. (a)–(d) Different capillary positions.
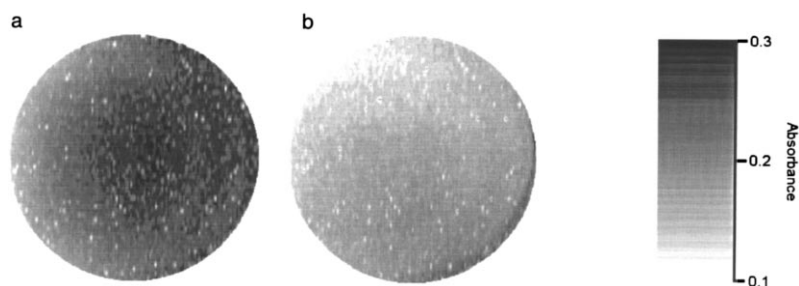
Fig. 8. Sb free atom distribution in the dual mode atomizer. Unheated flame-in-tube mode, 2100 ml min^{-1} H$_2$, 20 ml min O$_2$, 400 ng ml^{-1} Sb, wall alignment. (a) Properly centred capillary; (b) capillary off axis in the inlet arm.

concentration close to the atomizer's wall (Fig. 10a) proves that the decay of free atoms takes place at the surface as in the unheated atomizer.

The homogeneity of the distribution is even increased with lowering the purge gas flow rate. This is in agreement with the results for the FIAS atomizer described below, as the atomization conditions in both atomizers become quite similar. Similarly, at the lowest gas flow rate (130 ml min^{-1} H$_2$; flame-in-tube mode), calibration

rollover was observed at Sb concentrations over 600 ng ml^{-1} with non-homogeneous analyte distribution. This phenomenon will be treated in detail in Section 3.3.3.

3.3.3. The FIAS atomizer

The distribution of free atoms in the FIAS atomizer under typical experimental conditions, i.e. total gas flow rate around 100 ml min^{-1}, temperature 900°C, analyte concentration in the
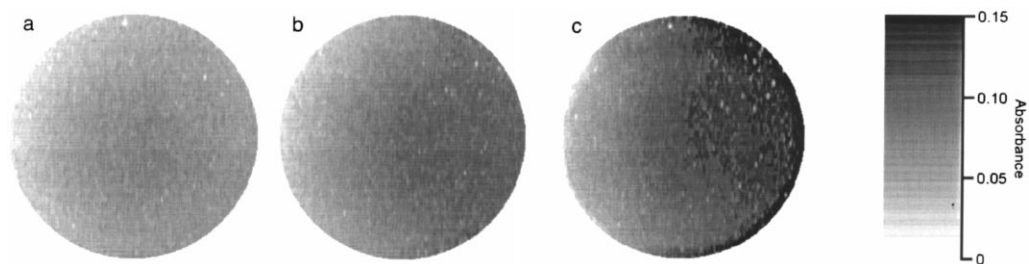

Fig. 9. Sb free atom distribution in the dual mode atomizer at low purge gas flow rates: 200°C, flame-in-tube mode, 20 ml min^{-1} O$_2$, 200 ng ml^{-1} Sb. (a) 430 ml min^{-1} H$_2$, (b) 230 ml min^{-1} H$_2$, (c) 130 ml min^{-1} H$_2$.
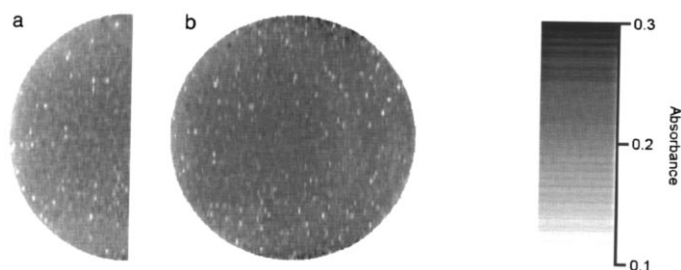

Fig. 10. Sb free atom distribution in the dual mode atomizer heated to 900°C, flame-in-tube mode: 2100 ml min^{-1} H$_2$, 20 ml min O$_2$, 400 ng ml^{-1} Sb. (a) Wall alignment, (b) centre alignment; and (c) absorbance in the horizontal band 10 pixels wide over the middle part of the tube.
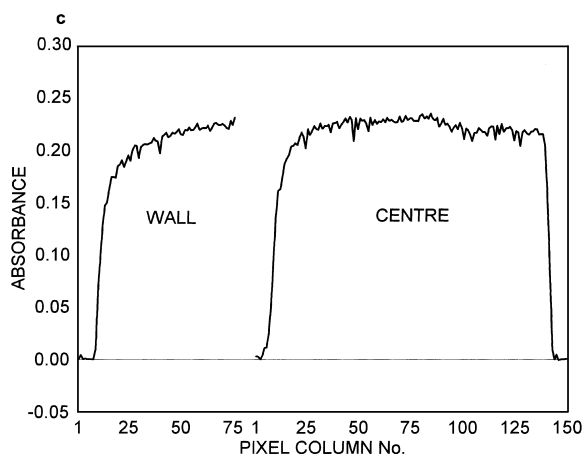
Fig. 10. *Continued*

ppb range, is homogeneous (see Fig. 11a). The dark stripe in the right part of the central picture is believed to be an artifact. Increasing the analyte concentration up to 200 ng ml^{-1}, absorbance increased to approximately 0.6 but the distribution is still homogeneous.

When the concentration of analyte was further increased to 300 ng ml^{-1}, the overall picture changed dramatically: absorbance decreased significantly and the free atom distribution became distinctly inhomogeneous (Fig. 11b). There was higher free atom density in the centre and especially close to the tube walls. It should be emphasized that the picture cannot be deformed by a non-specific absorption as checked at a neighbouring non-analytical line (259 nm). The situation corresponds to a calibration graph roll-over in the traditional, spatially unresolved, absorbance measurement. The roll-over was observed previously for selenium [19], antimony and arsenic [6] determinations in the same atomizer under analogous atomization conditions and for determination of selenium in other heated quartz atomizers at much higher purge gas flows [20]. Welz and Guo [6] found that the tendency to obtain roll-over was strongly amplified at conditions unfavourable for the formation of H-radicals. They concluded that the reason for the roll-over was incomplete free atom formation at higher concentrations because of a deficiency of hydrogen radicals, caused by a too high concentration of hydride consuming analyte species.

An alternative explanation for a similar roll-over condition in a modification of an unheated flame-in-tube atomizer was offered by D' Ulivo and Dědina [21]. They proved that the roll-over in their atomizer was not due to a depletion of H-radicals but due to complex reactions of analyte species taking place in the free volume of the
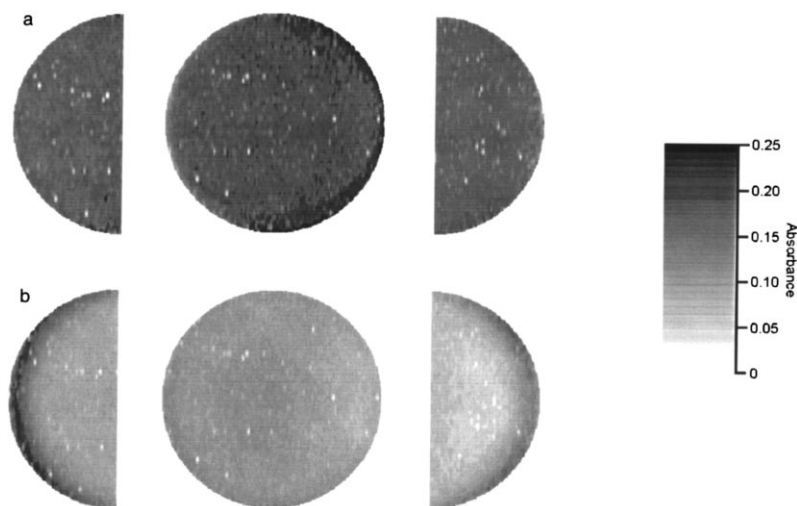

Fig. 11. Sb free atom distribution in the FIAS atomizer heated to 900°C: 50 ml min^{-1} Ar, 30 ml min^{-1} H$_2$. Left wall, centre and right wall alignment. (a) 50 ng ml^{-1} Sb; and (b) 300 ng ml^{-1} Sb.

atomizer: free selenium atoms combine to form dimers in a first step of a sequence of reactions which eventually lead to the formation of polyatomic particles. The removal of remaining free atoms is thus accelerated due to reactions on the reactive particle surfaces.

The free atom distribution shown in Fig. 11b, notably the higher absorbance near the tube axis, is difficult to explain by H-radical deficiency. It seems rather compatible with the above scheme of free analyte atom/particle reactions: When the atom density in the atomizer's atmosphere is increased above a certain limit, formation of dimers, polyatomic species and clusters begins, thus rapidly increasing the available reactive surface. This contributes to enhanced decay, manifesting itself in the calibration curvature and even roll-over. The higher free atom density in the centre could be ascribed to better prevention of particle formation since H-radical concentration in this region should be maximum there [1]. The increased density of free atoms near the walls indicates lower particle concentration there, which could be ascribed to particles sticking to the tube walls. Adsorbed particles probably create a metallic film which should subsequently evaporate mainly as dimers (according to thermodynamic equilibrium calculations [22]). No deposits within the tube nor memory effects were observed, although prolongation of signal tailing analogous to that observed in Welz and Guo [6] cannot be excluded. The prevention of particles in the centre and their removal close to the walls should create a pronounced particle concentration gradient within the tube because the rate of particle diffusion must be much slower than that of free atoms.

The existence of such particles was not directly proven here, e.g. by use of non-specific absorption or light scattering. More effort is needed in this direction, including the experiments with other hydride forming elements as the potential source of gaseous phase interferences proceeding via a similar mechanism.

4. Conclusions

From the practical point of view, negligible cross-sectional inhomogeneity was observed in the externally heated 'flameless' quartz tubes, which are the most widely used in analytical practice. Even less inhomogeneity would be expected with routinely used AAS instruments since they are configured in such a way that the radiation beam geometry is practically 'blind' to regions close to the walls of the quartz tube, i.e. where slight atom density gradients were observed. Consequently, no significant effects arising from free atom density gradients are to be expected in routine analysis.

References

[1] J. Dědina, D.L. Tsalev, Hydride Generation Atomic Absorption Spectrometry, Wiley, Chichester, 1995.

[2] J. Dědina, I. Rubeška, Hydride atomization in a cool hydrogen−oxygen flame burning in a quartz tube atomizer. Spectrochim. Acta Part B 35 (1980) 119−128.

[3] B. Welz, M. Melcher, Investigations on atomisation mechanisms of volatile hydride-forming elements in a heated quartz cell. Part 1. Gas-phase and surface effects; decomposition and atomisation of arsine. Analyst 108 (1983) 213−224.

[4] J. Dědina, Quartz tube atomizers for hydride generation atomic absorption spectrometry: mechanism of selenium hydride atomization and fate of free atoms. Spectrochim. Acta Part B 47 (1992) 689−700.

[5] J. Dědina, B. Welz, Quartz tube atomizers for hydride generation atomic absorption spectrometry: Fate of free arsenic atoms. Spectrochim. Acta Part B 48 (1993) 301−314.

[6] B. Welz, T.Z. Guo, Formation and interpretation of double peaks in flow injection hydride generation atomic absorption spectrometry. Spectrochim. Acta Part B 47 (1992) 645−658.

[7] M. Johansson, D.C. Baxter, K.E.A. Ohlsson, W. Frech, Mechanism of formation and spatial distribution of lead atoms in quartz tube atomizers. Spectrochim. Acta Part B 52 (1997) 643−656.

[8] S.G. Salmon, J.A. Holcombe, Optical system for gathering simultaneous time and spatial data from transient events. Anal. Chem. 51 (1979) 648−650.

[9] G.D. Rayson, J.A. Holcombe, Spatially resolved Arrhenius determinations within a graphite furnace atomizer. Spectrochim. Acta Part B 38 (1983) 987−993.

[10] J.D. Stafford, J.A. Holcombe, Time-gated resonance schlieren studies of analyte distribution in a graphite furnace atomizer. J. Anal. Atom. Spectrom. 3 (1988) 35−42.

[11] C.W. Huie, C.J. Curran, Spatial mapping of analyte distribution within a graphite furnace atomizer. Appl. Spectrosc. 42 (1988) 1307−1311.

[12] A.K. Gilmutdinov, Y.A. Zakharov, V.P. Ivanov, A.V. Voloshin, Shadow spectral filming: a method of investigating electrothermal atomization. Part 1. Dynamics of formation and structure of the absorption layer of thallium, indium, gallium and aluminium atoms. J. Anal. Atom. Spectrom. 6 (1991) 505−519.

[13] C.L. Chakrabarti, A.K. Gilmutdinov, J.C. Hutton, Digital imaging of atomization processes in electrothermal atomizers for atomic absorption spectrometry. Anal. Chem. 65 (1993) 716−723.

[14] T. Matoušek, J. Dědina, Mechanism of Interferences in Selenium Hydride Atomization in Quartz Tubes for AAS, Poster presented at CSI XXIX, Leipzig, 1995.

[15] J. Dědina, B. Welz, Quartz tube atomizers for hydride generation atomic absorption spectrometry — mechanism for atomization of arsine — invited lecture. J. Anal. Atom. Spectrom. 7 (1992) 307−314.

[16] A.K. Gilmutdinov, B. Radziuk, M. Sperling, B. Welz, Spatially and temporally resolved detection of analytical signals in graphite furnace atomic absorption spectrometry. Spectrochim. Acta Part B 51 (1996) 1023−1034.

[17] A.K. Gilmutdinov, T.M. Abdulina, S.F. Gorbachev, V.L. Makarov, Concentration curves in atomic absorption spectrometry. Spectrochim. Acta Part B 47 (1992) 1075−1095.

[18] J. Dědina, A. D' Ulivo, Argon shielded, highly fuel-rich, hydrogen−oxygen diffusion micro flame — a new hydride atomizer. Spectrochim. Acta Part B 52 (1997) 1737−1746.

[19] B. Welz, P. Stauss, Interferences of other hydride forming elements on selenium in hydride — generation atomic absorption spectrometry with a heated quartz tube atomizer. Spectrochim. Acta Part B 48 (1993) 951−976.

[20] J. Agterdenbos, J.P.M. Van Noort, F.F. Peters, D. Bax, The determination of selenium with hydride generation AAS-I. Description of the apparatus used and study of the reactions in the absorption cuvette. Spectrochim. Acta Part B 40 (1985) 501−515.

[21] A. D' Ulivo, J. Dědina, Interferences in hydride atomization studied by atomic absorption and atomic fluorescence spectrometry. Spectrochim. Acta Part B 51 (1996) 481−498.

[22] K. Dittrich, R. Mandry, C. Udelnow, A. Udelnow, Hydride atomization in graphite furnace atomizers. Fresenius J. Anal. Chem. 323 (1986) 793−799.